

Real-Time Optimization Strategies for Building Systems*

Victor M. Zavala

Mathematics and Computer Science Division

Argonne National Laboratory, 9700 South Cass Avenue, Argonne, IL 60439, USA

Abstract

We analyze different optimization strategies for real-time energy management in building systems. We have found that exploiting building-wide multivariable interactions between CO₂, humidity, pressure, occupancy, and temperature leads to significant reductions of energy intensity. Our analysis indicates that it is possible to obtain energy savings of more than 50% compared with traditional control strategies. The exploitation of the thermal comfort zone has been found to be the most relevant factor driving energy savings. We discuss strategies to handle multiple competing objectives as well as economic functions and we analyze financial incentives provided by real-time prices and existing market designs. Numerical experiments are provided to support the claims.

Keywords: building-wide, proactive, optimization, real-time, electricity markets, energy management.

1 Introduction

The heating, ventilation, and air-conditioning (HVAC) system comprises a large number of equipment units and material and energy resources that need to be monitored and coordinated in real time. The effective operation of these systems is particularly difficult because external and internal building conditions change in a highly dynamic manner. Such changes include, among others, occupancy, weather, and energy prices. In addition, building operations are complex because a large number of constraints must be satisfied in order to ensure comfort, air quality, and appropriate equipment performance.

Optimization-based control is a key technology in next-generation building systems. While diverse studies have been reported [16, 11, 12, 21, 4, 29, 18, 26], traditional control objectives (e.g., set-point tracking) are often used. In addition, previous studies have focused on independent components of the building such as air-handling units, chillers, ventilation rates, air quality, and temperature. Hence, the *building-wide* optimization potential has not been fully explored [3]. This is an issue because, in commercial-sized buildings, myriad operational degrees of freedom and physical multivariable interactions can be exploited to achieve significant energy savings.

*Preprint ANL/MCS-P1911-0611

Previous optimization studies have also focused on traditional interactions of the building with the electricity markets where the building is seen as a price-taker subject to price volatility or time of use tariffs. For instance, many optimization studies assume that demand shifting is the only strategy available to reduce electricity costs [4, 5]. The lack of understanding of the building physical potential and its interaction with electricity markets significantly limits the perceived value of building automation and thus its adoption.

The recent commercialization of proactive energy management technology has the potential of changing this landscape. These predictive control-based tools enable the anticipation of weather, occupancy trends and loads. This information can be used to compute economic-optimal set-point policies [29, 27, 30]. More importantly, predictive control is a multivariable strategy that can exploit the interactions between states and controls to optimize performance. The use of predictive models also makes buildings more adaptive to large dynamic fluctuations and enable a closer interaction with electricity markets. The energy and cost reduction potential of proactive energy management as well as the required optimization domain, however, have not been fully explored.

In this work, we analyze different strategies for *building-wide* optimization under a proactive framework. We demonstrate that building-wide strategies can exploit complex interactions between physical variables and their dynamics to achieve substantial energy savings without sacrificing air quality and comfort. Energy savings above 50% have been observed in our studies. We also consider strategies to handle competing objectives and adaptive constraints. In addition, we show that proactive strategies can be used to enable building participation in day-ahead and real-time electricity markets. This ability is key in reducing the exposure of buildings to real-time market volatility and can, in turn, lead to smoother operations. An interesting finding of this study was that energy minimization (as opposed to cost minimization) is a more reliable optimization strategy under variable prices with no financial incentives (e.g., strictly positive prices). This invalidates traditional perceptions that cost savings can only be accomplished through demand shifting strategies. In addition, it suggests that high prices alone might not provide enough incentives for demand reductions during peak times.

The paper is structured as follows. In Section 2 we present a physical dynamic model used to illustrate the optimization developments. In Section 3 we perform a degrees of freedom and constraint analysis. In Section 4 we discuss different optimization strategies, and in Section 5 we present a numerical case study. The paper closes in Section 6 with final remarks and directions of future work.

2 System Model

For our optimization studies, we consider a model describing the dynamics of a building space conditioned by an air-handling unit (AHU) system. The system is sketched in Figure 1. We capture the building conditions in terms of CO₂ concentration, humidity, pressure, and temperature. The model nomenclature is provided in Appendix A.

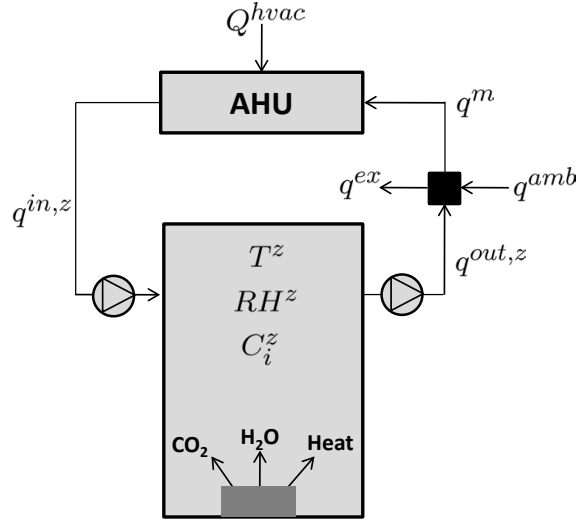


Figure 1: Schematic representation of building system [24].

2.1 Material Balances

In the building envelope we have the total mass balance,

$$\frac{dm^z(\tau)}{d\tau} = \rho \cdot (q^{in,z}(\tau) - q^{out,z}(\tau)), \quad (2.1)$$

where τ is time. We also have the component balances,

$$V^z \cdot \frac{dC_i^z(\tau)}{d\tau} = q^{in,z}(\tau) \cdot C_i^{in,z}(\tau) - q^{out,z}(\tau) \cdot C_i^z(\tau) + n(\tau) \cdot n_{tot} \cdot G_i^z, \quad i \in \{CO_2, H_2O\}. \quad (2.2)$$

Here, $n(\tau)$ is the occupancy signal of the space (value of one if the space is occupied and zero if it is unoccupied). The total number of occupants under occupied mode is given by n_{tot} . Assuming constant density and heat capacity in the mixer, we have

$$q^{out,z}(\tau) + q^{amb}(\tau) = q^{ex}(\tau) + q^m(\tau) \quad (2.3a)$$

$$C_i^z(\tau) \cdot q^{out,z}(\tau) + C_i^{amb}(\tau) \cdot q^{amb}(\tau) = C_i^z(\tau) \cdot q^{ex}(\tau) + C_i^m \cdot q^m(\tau), \quad i \in \{CO_2, H_2O\}. \quad (2.3b)$$

In the AHU, we have the following balances:

$$q^{z,in}(\tau) = q^m(\tau) \quad (2.4a)$$

$$m_i^{rm}(\tau) = q^{in,z}(\tau) \cdot C_i^{in,z}(\tau) - q^m(\tau) \cdot C_i^m(\tau), \quad i \in \{CO_2, H_2O\}. \quad (2.4b)$$

where m_i^{rm} are the mass removal rates with $m_{CO_2}^{rm}(\cdot) = 0$ since this component is not removed in the AHU. The relationship between the total building pressure, mass, and temperature can be estimated from the ideal gas law:

$$P^z(\tau) = \frac{m^z(\tau) \cdot R \cdot T^z(\tau)}{M \cdot V^z}. \quad (2.5)$$

We convert the relative humidity of the air at the building temperature $T^z(\tau)$ to volumetric concentration $C_{H_2O}^z(\tau)$ using the following relationship

$$RH^z(\tau) = 100 \cdot \frac{C_{H_2O}^z(\tau)}{C_{H_2O}^{sat}(\tau)}, \quad (2.6)$$

where the saturation concentration is given by Antoine's equation [23]

$$\log_{10}(C_{H_2O}^{sat}(\tau)) = 8.07131 - \frac{1730.63}{T^z(\tau) - 39.73}. \quad (2.7)$$

We can convert the volumetric concentration of CO_2 to ppmV (typical metric for air quality) using the relationship [1],

$$ppmV_{CO_2}^z(\tau) = 1000 \cdot \frac{C_{CO_2}^z(\tau) \cdot R \cdot T^z(\tau)}{M_{CO_2} \cdot P^z(\tau)}. \quad (2.8)$$

As can be seen, there exist interactions between the building physical variables. In particular, both the relative humidity and ppmV of CO_2 are affected by the building temperature. In addition, ppmV is affected by pressure.

2.2 Energy Balances

We consider the following energy balance for the building envelope [24]:

$$m^z(\tau) \cdot c_p \cdot \frac{dT^z(\tau)}{dt} = q^{in,z}(\tau) \cdot \rho \cdot c_p \cdot T^{in,z}(\tau) - q^{out,z}(\tau) \cdot \rho \cdot c_p \cdot T^z(\tau) - U^w \cdot A^w \cdot (T^z(\tau) - T^{amb}(\tau)) + n(\tau) \cdot n_{tot} \cdot Q^z. \quad (2.9)$$

In the mixer we have

$$q^{out,z}(\tau) \cdot T^z(\tau) + q^{amb}(\tau) \cdot T^{amb}(\tau) = q^{ex}(\tau) \cdot T^z(\tau) + q^m(\tau) \cdot T^m(\tau). \quad (2.10)$$

The amount of condensate in the AHU is proportional to the latent energy removed/added,

$$Q^{lat}(\tau) = h^{lat} \cdot m_{H_2O}^{rm}(\tau). \quad (2.11)$$

The amount of sensible energy removed/added in the AHU is given by

$$Q^{sens}(\tau) = q^{in,z}(\tau) \cdot \rho \cdot c_p \cdot (T^{in,z}(\tau) - T^m(\tau)). \quad (2.12)$$

The total energy consumed by the HVAC system is given by

$$Q^{hvac}(\tau) = |Q^{lat}(\tau)| + |Q^{sens}(\tau)|, \quad (2.13)$$

For computational efficiency, we replace the non-differentiable absolute value operator $|\cdot|$ using dummy variables as

$$Q^{hvac}(\tau) = Q_+^{lat}(\tau) + Q_-^{lat}(\tau) + Q_+^{sens}(\tau) + Q_-^{sens}(\tau) \quad (2.14a)$$

$$Q^{lat}(\tau) = Q_+^{lat}(\tau) - Q_-^{lat}(\tau) \quad (2.14b)$$

$$Q^{sens}(\tau) = Q_+^{sens}(\tau) - Q_-^{sens}(\tau), \quad (2.14c)$$

with $Q_+^{lat}(\tau), Q_-^{lat}(\tau), Q_+^{sens}(\tau), Q_-^{sens}(\tau) \geq 0$.

3 Degrees of Freedom and Constraint Analysis

If we assumed a fixed pressure $P^z(\tau) = P^z$ we have that $q^{in,z}(\tau) = q^{out,z}(\tau)$ so that $m^z(\tau)$ is constant and $q^{amb}(\tau) = q^{ex}(\tau)$. In this case, the system has three operational degrees of freedom. The first degree of freedom can be either $q^{amb}(\tau)$ or $q^{ex}(\tau)$ but not both. The other two degrees of freedom can be the supply air temperature $T^{in,z}(\tau)$ or $Q^{sens}(\tau)$ and the supply air humidity or $Q^{lat}(\tau)$. If we relax the constant pressure constraint through a *soft constraint* of the form

$$P_L \leq P(\tau) \leq P_U, \quad (3.15)$$

then the system has four degrees of freedom. This additional flexibility can be used to aid optimization. Therefore, we highlight that *the use of soft constraints in variables such as temperature, pressure, humidity, CO₂ and flow rates* maximizes optimization flexibility of the energy management system. This implies that the use of *fixed set-point conditions can dramatically limit the energy savings potential*.

To maximize flexibility, we propose to use soft constraints with set-back conditions as opposed to traditional strategies that use set-points with set-back conditions. To ensure comfort, we will make use of temperature and humidity constraints of the form:

$$T_L^z \cdot n(\tau) + (1 - n(\tau)) \cdot T_L^{z, sb} \leq T^z(\tau) \leq T_U^z \cdot n(\tau) + (1 - n(\tau)) \cdot T_U^{z, sb} \quad (3.16a)$$

$$RH_L^z \cdot n(\tau) + (1 - n(\tau)) \cdot RH_L^{z, sb} \leq RH^z(\tau) \leq RH_U^z \cdot n(\tau) + (1 - n(\tau)) \cdot RH_U^{z, sb}. \quad (3.16b)$$

Here, $T_L^z, RH_L^z, T_U^z, RH_U^z$ are nominal lower and upper bounds under occupied conditions and $T_L^{z, sb}, RH_L^{z, sb}, T_U^{z, sb}, RH_U^{z, sb}$ are bounds under set-back conditions. These *adaptive* constraints indicate that, when the building envelope is occupied at time τ , then $n(\tau) = 1$, and nominal bounds will be imposed. On the other hand, if the envelope is not occupied, then *set-back bounds* will be imposed.

An alternative way of measuring comfort is using the predicted mean vote (PMV) and predicted percentage dissatisfied (PPD) indexes [20]. If a PPD prediction model is incorporated, then adaptive constraints on PPD of the form (3.16) can be imposed in the same way. This provides an advantage since PPD is a more direct comfort metric. PPD models, however, are complex and difficult to handle by optimization solvers. Consequently, this will be left as a subject of future work. The generality of concepts presented, however, still apply.

We consider constraints on air quality of the form

$$ppmV_{CO_2}^z(\tau) \leq ppmV_{CO_2,U}^z \cdot n(\tau) + (1 - n(\tau)) \cdot ppmV_{CO_2,U}^{z, sb}. \quad (3.17)$$

The use of such constraint assumes that CO₂ concentration can be measured or inferred. In the absence of such information, an indirect strategy to ensure air quality is to impose constraints on the total ambient air flow rate (ventilation) as a function of the number of occupants:

$$q^{amb}(\tau) \geq q_{oc}^{amb} \cdot n(\tau) \cdot n_{tot} + (1 - n(\tau)) \cdot q_L^{amb, sb}. \quad (3.18)$$

Here, q_{oc}^{amb} is the minimum flow rate per occupant as dictated by ASHRAE [15] and $q_L^{amb, sb}$ is a set-back bound set under unoccupied conditions. Imposing constraints directly on CO₂ concentration is desirable as more flexible ventilation constraints of the form $q_L^{amb} \leq q^{amb} \leq q_U^{amb}$ can be used. Here, q_L^{amb}, q_U^{amb} are the *physical limits* of ventilation.

Dampers represent an important dynamic constraint due to their slow dynamics. In other words, they cannot be moved freely because of physical limitations or equipment wearing. This can be modeled by using *ramp* constraints of the form,

$$\left| \frac{dq^{in,z}(\tau)}{d\tau} \right| \leq \Delta q_U^{in,z} \quad (3.19a)$$

$$\left| \frac{dq^{out,z}(\tau)}{d\tau} \right| \leq \Delta q_U^{out,z} \quad (3.19b)$$

$$\left| \frac{dq^m(\tau)}{d\tau} \right| \leq \Delta q_U^m \quad (3.19c)$$

$$\left| \frac{dq^{amb}(\tau)}{d\tau} \right| \leq \Delta q_U^{amb} \quad (3.19d)$$

$$\left| \frac{dq^{ex}(\tau)}{d\tau} \right| \leq \Delta q_U^{ex}. \quad (3.19e)$$

We also impose operational bounds on the AHU delivery temperature (since it might affect equipment performance and comfort) and physical bounds on the flow rates,

$$T_L^{in,z} \leq T^{in,z}(\tau) \leq T_U^{in,z} \quad (3.20a)$$

$$q_L^{in,z} \leq q^{in,z}(\tau) \leq q_U^{in,z} \quad (3.20b)$$

$$q_L^{out,z} \leq q^{out,z}(\tau) \leq q_U^{out,z} \quad (3.20c)$$

$$q_L^{ex} \leq q^{ex}(\tau) \leq q_U^{ex} \quad (3.20d)$$

$$q_L^m \leq q^{amb}(\tau) \leq q_U^m. \quad (3.20e)$$

Finally we consider initial conditions for the dynamic states of the system,

$$m^z(t) = m_{init}^z \quad (3.21a)$$

$$T^z(t) = T_{init}^z \quad (3.21b)$$

$$C_i^z(t) = C_{i,init}^z, \quad i \in \{CO_2, H_2O\}. \quad (3.21c)$$

4 Proactive Energy Management

Buildings are operated under different performance objectives (economic vs. environmental), pricing structures, and interactions with electricity markets. Thus, different optimization formulations can be envisioned. In this section, we consider some basic formulations.

4.1 Energy Minimization

We first consider a building-wide energy minimization optimal control formulation (i.e., with *fixed prices*) over the time interval $\tau \in [t, t + T]$:

$$\min \Phi_1 \quad (4.22a)$$

$$\text{s.t. (2.1) - (3.21), } \tau \in [t, t + T], \quad (4.22b)$$

where

$$\Phi_1 = \int_t^{t+T} Q^{hvac}(\tau) d\tau. \quad (4.23)$$

This is a direct building-wide strategy that can fully exploit the multivariable interactions of the building and HVAC system.

For the sake of comparison, we consider a standard approach that uses set-points with set-back conditions to save energy and uses controllers to track these set-points as tightly as possible [18, 19, 7, 6]. This leads to the following formulation:

$$\min \Phi_1 \quad (4.24a)$$

$$\text{s.t. (2.1) – (3.21), } \tau \in [t, t + T], \quad (4.24b)$$

where,

$$\begin{aligned} \Phi_1 = \int_t^{t+T} & (\|T^z(\tau) - T^{sp}(\tau)\|^2 + \|RH^z(\tau) - RH^{sp}(\tau)\|^2 \\ & + \|P^z(\tau) - P^{sp}(\tau)\|^2 + \|ppmV_{CO_2}^z(\tau) - ppmV_{CO_2}^{sp}(\tau)\|^2) d\tau. \end{aligned} \quad (4.25)$$

The set-points are given by

$$T^{sp}(\tau) = \bar{T} \cdot n(\tau) + (1 - n(\tau)) \cdot \bar{T}^{sb} \quad (4.26a)$$

$$RH^{sp}(\tau) = \bar{RH} \cdot n(\tau) + (1 - n(\tau)) \cdot \bar{RH}^{sb} \quad (4.26b)$$

$$P^{sp}(\tau) = \bar{P} \cdot n(\tau) + (1 - n(\tau)) \cdot \bar{P}^{sb} \quad (4.26c)$$

$$ppmV_{CO_2}^{sp}(\tau) = ppm\bar{V}_{CO_2} \cdot n(\tau) + (1 - n(\tau)) \cdot ppm\bar{V}_{CO_2}^{sb}. \quad (4.26d)$$

Here, \bar{T} , \bar{RH} , \bar{P} , $ppm\bar{V}_{CO_2}$ are the set-points under occupied conditions, and \bar{T}^{sb} , \bar{RH}^{sb} , \bar{P}^{sb} , $ppm\bar{V}_{CO_2}^{sb}$ are the set-points for unoccupied (set-back) conditions. A problem with this strategy is that the optimal set-back points depend on the building internal and external conditions which are highly dynamic. In addition, imposing set-points indirectly fixes operational variables. In Section 5 we will show that this rigidity leads to significantly more energy consumption compared with the building-wide strategy.

4.2 Handling Competing Objectives

Minimizing costs is not equivalent to minimizing energy or maximizing comfort. Typically, competing objectives like these arise in practice. In the presence of two competing objectives, problem (4.22) becomes a multi-objective problem of the form [8]

$$\min \{\Phi_1, \Phi_2\} \quad (4.27a)$$

$$\text{s.t. (2.1) – (3.21), } \tau \in [t, t + T]. \quad (4.27b)$$

We will define the objective vector $\Phi^T = [\Phi_1, \Phi_2]^T$. A practical strategy to handle multiple objectives in real-time consists in identifying the *utopia point* and to operate as close as possible to it [14].

To identify the utopia point, we solve problem (4.22) for each objective separately. This gives the cost functions $\Phi_L^T = [\Phi_1^L, \Phi_2^L]^T$, which are the coordinates of the utopia point. The nearest point to the utopia along the Pareto front (compromise solution) is determined by solving the following problem:

$$\min \|\Phi - \Phi^L\|_p := \left(\sum_{i=1,2} |\Phi_i - \Phi_i^L|^p \right)^{\frac{1}{p}} \quad (4.28a)$$

$$\text{s.t. (2.1) - (3.21), } \tau \in [t, t + T]. \quad (4.28b)$$

Here, $\|\cdot\|_p$ is the p-norm. The approach is illustrated in Figure 2. The utopia-tracking strategy provides advantages over traditional weighting objectives of the form [27],

$$\min w_1 \cdot \Phi_1 + w_2 \cdot \Phi_2 \quad (4.29a)$$

$$\text{s.t. (2.1) - (3.21), } \tau \in [t, t + T], \quad (4.29b)$$

since the weights have to be tuned as the building conditions change. The utopia following strategy also avoids the need to construct the Pareto front at each point in time, which is prohibitively expensive. For instance, in Figure 2, we can see that the Pareto front becomes steep and difficult to compute when Φ_2 approaches Φ_2^L .

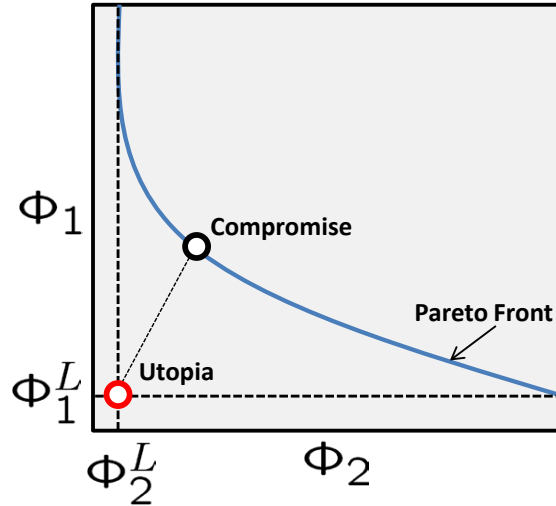


Figure 2: Schematic representation of utopia-tracking approach.

If we consider a trade-off between energy consumption Φ_1 and thermal comfort, we can consider a competing comfort objective of the form

$$\Phi_2 = \int_t^{t+T} (\|T^z(\tau) - T^{com}(\tau)\|^2 + \|RH^z(\tau) - RH^{com}(\tau)\|^2) d\tau. \quad (4.30)$$

where $T^{com}(\tau)$ and $RH^{com}(\tau)$ are the desired comfort point under occupied and unoccupied conditions for temperature and relative humidity, respectively. These have the form in (4.26). If a PPD

metric is used to measure comfort, then PPD can be used directly as the competing objective. We note that ensuring comfort using set-points is a more rigid approach than using the comfort zone constraints (3.16). Consequently, we will only use the set-point tracking approach for the sake of comparison.

4.3 Economic Objectives

In this section, we consider strategies to optimize building economic performance under two general settings. The first assumes that the building is a price taker, so it follows prices from the utility company or independent system operator (ISO). In the second paradigm, the building is assumed to be a consumer that bids into the day-ahead market to lock its demand in order to mitigate risk and avoid volatility in real-time prices.

4.3.1 Price Taking

If the building is charged real-time (spot) prices, the cost minimization problem takes the form

$$\min \Phi_1 \tag{4.31a}$$

$$\text{s.t. (2.1) – (3.21), } \tau \in [t, t + T], \tag{4.31b}$$

where,

$$\Phi_1 = \int_t^{t+T} \lambda(\tau) \cdot Q^{hvac}(\tau) d\tau. \tag{4.32}$$

Here, $\lambda(\tau)$ are the time-varying spot prices.

4.3.2 Day-Ahead and Real-Time Bidding

Proactive optimization strategies can use the dynamic building model to forecast the demand over the next day and bid into electricity markets. This information can be used to lock demands in day-ahead markets and thus avoid volatile prices (e.g., at peak times) in real-time markets. The use energy management strategies that respond to volatile real-time prices can lead to significant equipment wearing as well as economic inefficiency and constraint violations due to the limited dynamic responsiveness of the building.

In Figure 3 we present day-ahead and real-time wholesale prices at the Illinois hub of Midwest ISO in 2009. The figure clearly shows that real-time prices are significantly more volatile. In addition, real-time prices become often negative, providing incentives for consumers to increase energy demands.

To deal with the day-ahead bidding problem, we consider a supply function of the form

$$Q^{hvac}(\tau) = \alpha(\tau) - \beta(\tau) \cdot \lambda(\tau). \tag{4.33}$$

Here, the objective is to determine the optimal parameters $\alpha(\tau), \beta(\tau) \geq 0$ that maximize profit under the expected *day-ahead price* trajectory $\lambda(\tau)$. The parameter $\beta(\tau)$ is the demand elasticity, and $\alpha(\tau)$ is

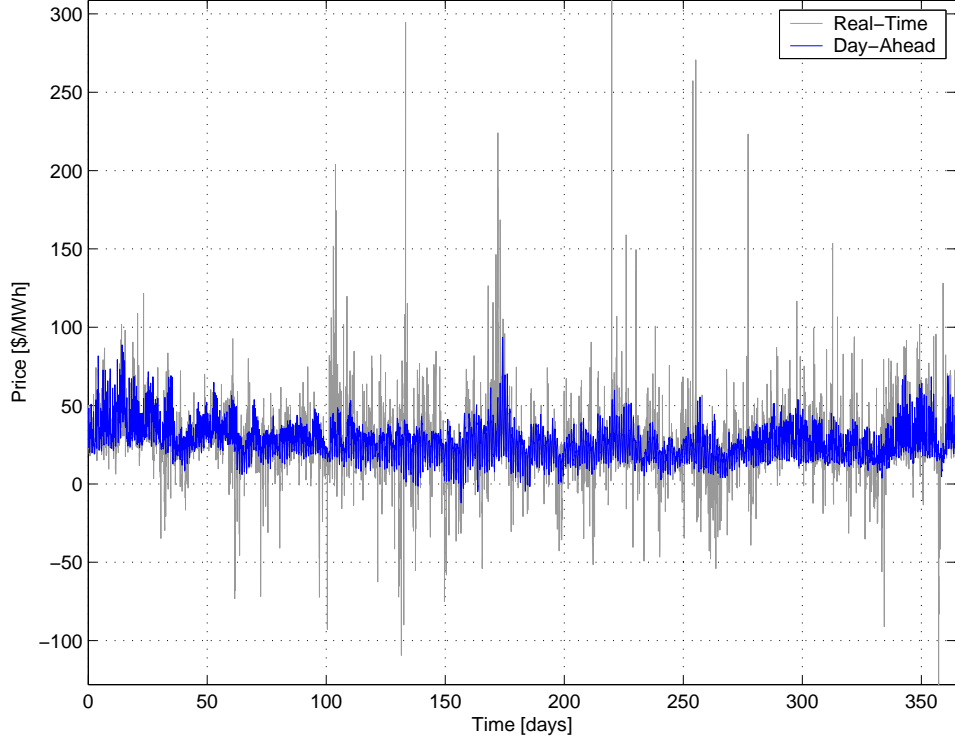


Figure 3: Day-ahead and real-time prices at Illinois hub of Midwest ISO in 2009.

a nominal demand. These parameters can be obtained by solving the following problem:

$$\min \int_t^{t+T} \lambda(\tau) \cdot Q^{hvac}(\tau) d\tau \quad (4.34a)$$

$$\text{s.t. (2.1) – (3.21), } \tau \in [t, t+T] \quad (4.34b)$$

$$Q^{hvac}(\tau) = \alpha(\tau) - \beta(\tau) \cdot \lambda(\tau), \tau \in [t, t+T] \quad (4.34c)$$

$$\alpha(\tau), \beta(\tau) \geq 0, \tau \in [t, t+T]. \quad (4.34d)$$

Once the bidding parameters are sent to the ISO, the ISO clears the market at the day-ahead prices $\lambda_D(\tau)$ and schedules the demand $Q_D^{hvac}(\tau)$ that the building should follow during the day. Any deviations from the schedule will be charged at real-time prices, which we define as $\lambda_R(\tau)$. Consequently, we consider minimizing the integral of the penalty costs,

$$\min \int_t^{t+T} \lambda_R(\tau) \cdot |Q^{hvac}(\tau) - Q_D^{hvac}(\tau)| d\tau. \quad (4.35a)$$

$$\text{s.t. (2.1) – (3.21), } \tau \in [t, t+T]. \quad (4.35b)$$

4.4 Real-Time Implementation and Computational Issues

For real-time implementation, the building optimization problem can be solved in a receding-horizon manner (see Figure 4). This enables the system to handle model and forecast errors. It is done at

preselected intervals Δ and with a prediction horizon T . At time t , the problem is solved over horizon $[t, t + T]$, and the resulting dynamic set-point policies (e.g., temperature, humidity, ventilation) are sent to the low-level controllers for tracking during period $[t, t + \Delta]$. At the next time $t + \Delta$ the prediction horizon is shifted to $[t + \Delta, t + \Delta + T]$, and the process is repeated to updated the policies, thus closing the loop. The length of the prediction horizon should be long enough to capture the periodicity of the building forcings such as weather and prices [30, 29].

From a computational point of view, we note that building-wide optimization problems can become large and nonlinear. To solve these problems, we recommended to use discretization approaches coupled to sparse optimization solvers. These approaches are highly efficient and are capable of solving problems with several hundreds of differential and algebraic equations in a few seconds. In particular, the use of *open* equation-oriented models is beneficial from a computational point of view since exact derivative information can be exploited to accelerate solutions. For a review of these methods, we refer the reader to [28, 10]. Equation-oriented strategies are significantly more efficient than traditional simulation-based approaches that use black-box simulation engines such as EnergyPlus [9] or TRNSYS [17].

The optimization strategies presented here used an implicit Euler discretization scheme and were implemented on the equation-oriented modeling system AMPL [13]. The resulting nonlinear optimization problems were solved with the sparse solver IPOPT [25]. Each *year-round* simulation took, on average, 3 minutes to complete on a standard personal computer. This illustrates the efficiency of the strategy. All models and software routines are available at <http://www.mcs.anl.gov/~vzavala/publications.html>.

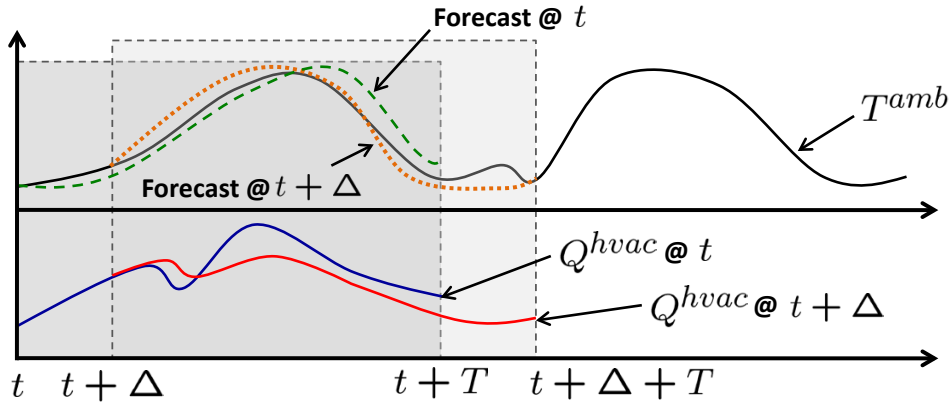


Figure 4: Schematic representation of receding-horizon implementation.

5 Numerical Analysis

We illustrate the concepts presented through year-round receding-horizon simulations under real ambient conditions at a location in the U.S. Midwest. Hourly profiles for ambient temperature and relative humidity were generated by using the weather forecasting system WRF available at Argonne

National Laboratory [29]. The profiles are presented in Figure 5. It is notable the high variability of weather at this region. For instance, during seasonal transitions, ambient temperature can vary by over 20°C in a single day. This variability has provided valuable information to assess the performance of the different optimization strategies.

In all our numerical experiments we assume an ambient concentration of CO_2 of 400 ppmV. In addition, we will assume an occupancy schedule of 8 a.m. to 6 p.m. during weekdays. We consider a commercial-sized building with a volume of $1,000\text{ m}^3$ and 500 occupants.

We highlight that the overall magnitude of the savings presented in the following analysis is system and climate dependent and should be taken with care. The analysis presented tries to explain general trends in behavior.

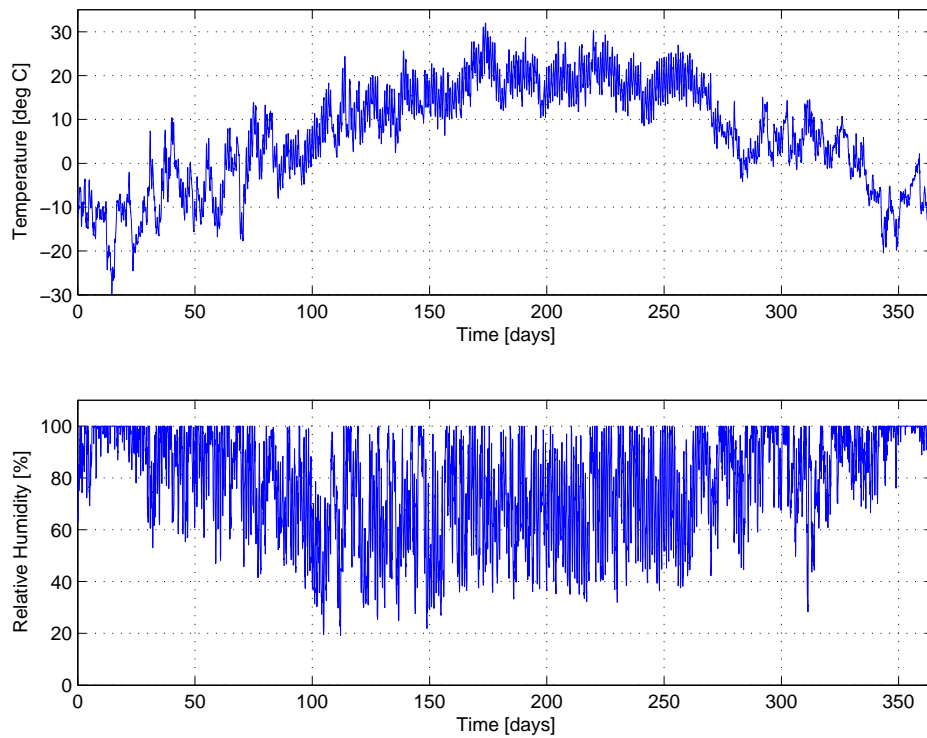


Figure 5: Ambient conditions for numerical study.

5.1 Energy Savings

In this section we compare the energy savings performance of the proposed building-wide optimization with that of a standard set-point strategy. In addition, we analyze the impact on savings and flexibility of different constraints.

5.1.1 Set-Point Tracking vs. Building-Wide Optimization

We first compute the energy consumption of a set-point tracking strategy with set-back mode conditions (4.24). In this case, the set-back temperature set-points are chosen as the ambient conditions and we impose temperature limits of 10-30°C. The set-point under occupied conditions was set to 23°C. We assumed a relative humidity set-point of 50% and a pressure set-point of 1 atm. In this experiment we assumed a variable ventilation rate (no occupant-dependent) with a CO₂ limit of 1,000 ppmV.

The year-round results are presented in Figure 6. In the top graph, we can see the fluctuations in the building temperature from the normal set-point to the set-back set-point during different seasons. We can see that, during winter, the system moves to the lower limit of 10°C at night while during summer it moves to 30°C. The year-round energy consumption for this case was 1,530 MWh. We can note that a large amount of energy is wasted during unoccupied periods specially during winter since the system is trying to keep the temperature at the lower limit without realizing that it can close ventilation to do so. In other words, the use of tracking objectives *wastes the operational flexibility of the building*.

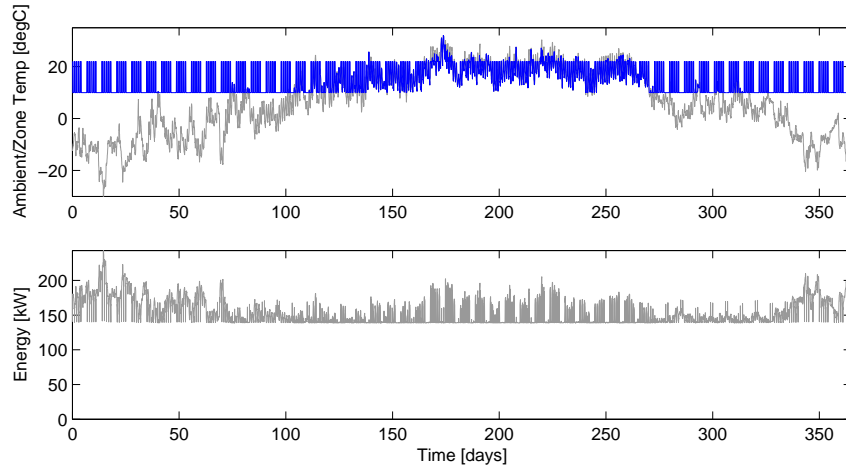


Figure 6: Temperature (top) and energy consumption (bottom) profile for tracking strategy.

We now consider the building-wide strategy for direct energy minimization (4.22). In this strategy, the building temperature is allowed to fluctuate within the adaptive comfort zone given by the constraints (3.16). In this case, the comfort zone in occupied mode is assumed to be 21 – 27°C for temperature and 30 – 50% for humidity. This range was selected to keep a percentage of people dissatisfied (PPD) level of less than 15% [20]. At all times, a pressure of 1 atm was maintained. During unoccupied conditions, the building temperature and humidity were relaxed to 10-30°C and 20-70%, respectively.

The results are presented in Figure 7. As can be seen, the building-wide strategy exploits the comfort zone more often during the year. The optimized profiles follow nonintuitive patterns during seasonal transitions which differ from those of the tracking strategy with set-back conditions. This

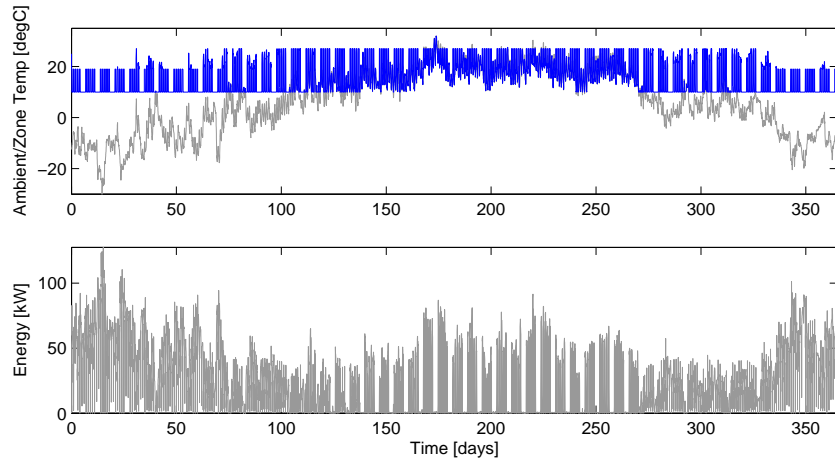


Figure 7: Temperature (top) and energy consumption (bottom) profile for building-wide optimization strategy.

stresses the need to optimize the building in an adaptive manner. The building-wide approach exploits the unoccupied periods to minimize energy, dropping the energy consumption to almost zero during unoccupied conditions by making use of ventilation. In addition, the system anticipates the building closing time to minimize energy and delay the temperature to unoccupied times. The year-round energy consumption in this scenario was 230 MWh. The building-wide strategy consumes 5 times less energy than the set-point tracking strategy (a relative reduction of 85%).

Another interesting feature of the building-wide system is that it exploits the ambient temperature conditions to optimize the AHU delivery temperature. This point is highlighted in Figure 8 where we compare the AHU delivery temperature policies (T_{in}^z) for the building-wide and tracking strategies. Note that the building-wide strategy follows a much different pattern and exploits the entire range. It has been found that energy optimizing AHU delivery temperature is one of the key degrees of freedom that can be used to save energy. This is consistent with existing practical experience [30].

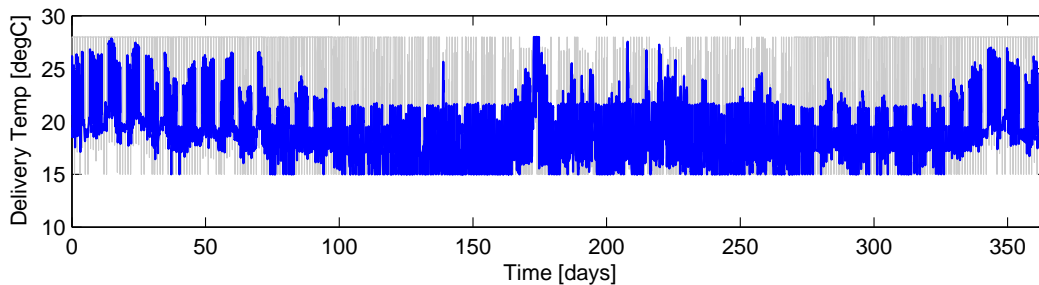


Figure 8: Delivery temperature of air handling unit under tracking (dark line) and building-wide (light line) optimization strategies.

A key conclusion from this first analysis is that exploiting the building flexibility (e.g., entire

operational limits) is critical to achieve significant savings. In the following sections, we demonstrate that the *exploitation of the thermal comfort zone* is the most relevant factor. This is done by analyzing the impact of different degrees of freedom and constraints on energy savings.

5.1.2 Effects of Ventilation

Ventilation rates ($q^{amb}(\tau)$ in the model) are usually set around 5 cfm ($8 \text{ m}^3/\text{hr}$) per occupant in office buildings. It is well known that fixed ventilation rates can significantly limit the economic performance of the building [15].

In Figure 9, we present the energy consumption for the building-wide strategy under different fixed ventilation rates and the resulting maximum CO₂ concentration observed in the building during the year. The maximum ventilation rate $4,000 \text{ m}^3/\text{hr}$ is the rate corresponding to 500 occupants and using an estimate of $8 \text{ m}^3/\text{hr}$ per occupant. The corresponding year-round energy consumption was 277 MWh with a maximum CO₂ concentration of 800 ppmV. The minimum ventilation rate used was $100 \text{ m}^3/\text{hr}$ which leads to an energy consumption of 228 MWh. This rate, however, leads to a maximum CO₂ concentration of 5,000 ppmV, which is clearly not acceptable.

As expected, there is a clear trade-off between ventilation and energy. The trade-off exists because the building-wide strategy tries to *seal the building envelope* in order to preserve energy. In other words, increasing continuous ventilation wastes the energy used for conditioning the building envelope. However, in Figure 9 we can observe a flat surface in which the maximum CO₂ concentration does not change as the ventilation rate is increased (energy consumption, however, keeps increasing). This clearly illustrates that *fixed ventilation rates are highly conservative*. This points out the need to have adaptive estimates of minimum ventilation rates. In this scenario, for instance, the ventilation rate can be decreased to a value as low as $1,500 \text{ m}^3/\text{hr}$ to reduce energy from 277 MWh to 230 MWh (17% reduction) without crossing the 1,000 ppmV threshold. We also observe that decreasing the ventilation rate beyond this point does not decrease energy significantly (the savings for a rate of $100 \text{ m}^3/\text{hr}$ are 18%) but the maximum CO₂ increases exponentially. We have found that a limiting value of 25% savings (relative to 277 MWh) would require ventilation rates of $10 \text{ m}^3/\text{hr}$ or less. At this regime, the energy losses through the building walls dominate. On the other side of the curve, we can see that an overestimation of about 10% on ASHRAE's suggested ventilation rate ($4,500 \text{ m}^3/\text{hr}$) can increase energy to 300 MWh, decreasing energy savings to 80%.

Notably, even with ASHRAE's limits in ventilation, the savings of the building-wide strategy compared with the tracking strategy are 82%. This indicates that it is the combined effect of comfort zone exploitation and an efficient estimation of ventilation leading to energy savings. In addition, the magnitude of the change suggests that comfort zone exploitation is a more relevant factor.

Typically, fixed ventilation rates are used because of the lack of sensors to determine the number occupants and the actual CO₂ concentration in the building. We consider an alternative in which we use directly constraints on CO₂ concentration (1,000 ppmV during occupied times and 1,500 ppmV under unoccupied times) as an alternative to fixed ventilation rates. The year-round energy consumption was 220 MWh for this case which represents reduction of 20% with respect to the 277 MWh obtained with a maximum ventilation rate of $4,000 \text{ m}^3/\text{hr}$.

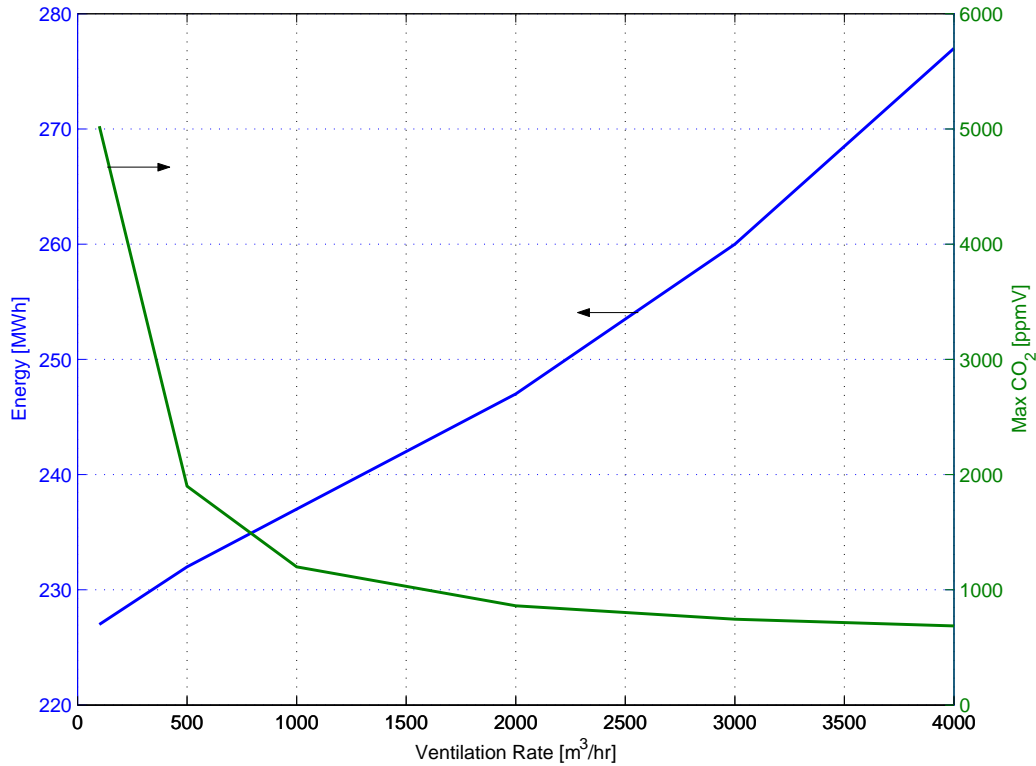


Figure 9: Effect of ventilation rates on year-round energy consumption and CO₂ concentration.

The profiles for CO₂ concentration and ventilation rates (ambient flow) are presented in Figure 10. As can be seen, the building-wide strategy satisfies the bounds during occupied times and it relaxes them during unoccupied times reaching levels of around 1,400 ppmV (note the double frequency signal). The fact that generation of CO₂ is not observed during unoccupied periods suggests that the optimization strategy decreases the ventilation rate prior to the transition to unoccupied mode in the afternoon. Thus, the slow CO₂ dynamics (the total air mass in the envelope is around one metric ton) can be exploited to save energy while satisfying the CO₂ limits during occupied times. This can be clearly observed in Figure 11 where we present a close-up during a week of operation. In the middle graph we can see that the building is sealed almost entirely for one hour during occupied mode, generating a *delayed* spike in the CO₂ concentration (three hours later) during the unoccupied period with relaxed CO₂ constraints. The strong periodicity of the ventilation rates and CO₂ concentration suggests that the occupancy pattern drives energy consumption. In the top graph of Figure 11 we can also observe that the building saves energy during the weekend by sealing the building almost entirely. This results in a very slow decay of the CO₂ concentration. This analysis illustrates that the slow dynamics of CO₂ and not only the temperature dynamics play an important role.

An unexpected result that we have obtained is that tightening the bounds on CO₂ to levels of 700 ppmV does not increase energy consumption as long as the ventilation rate is allowed to move freely. This observation is significant because it implies that *high air quality can be achieved without having high ventilation rates*. From equation (2.8) we can see that temperature and pressure can be used to control

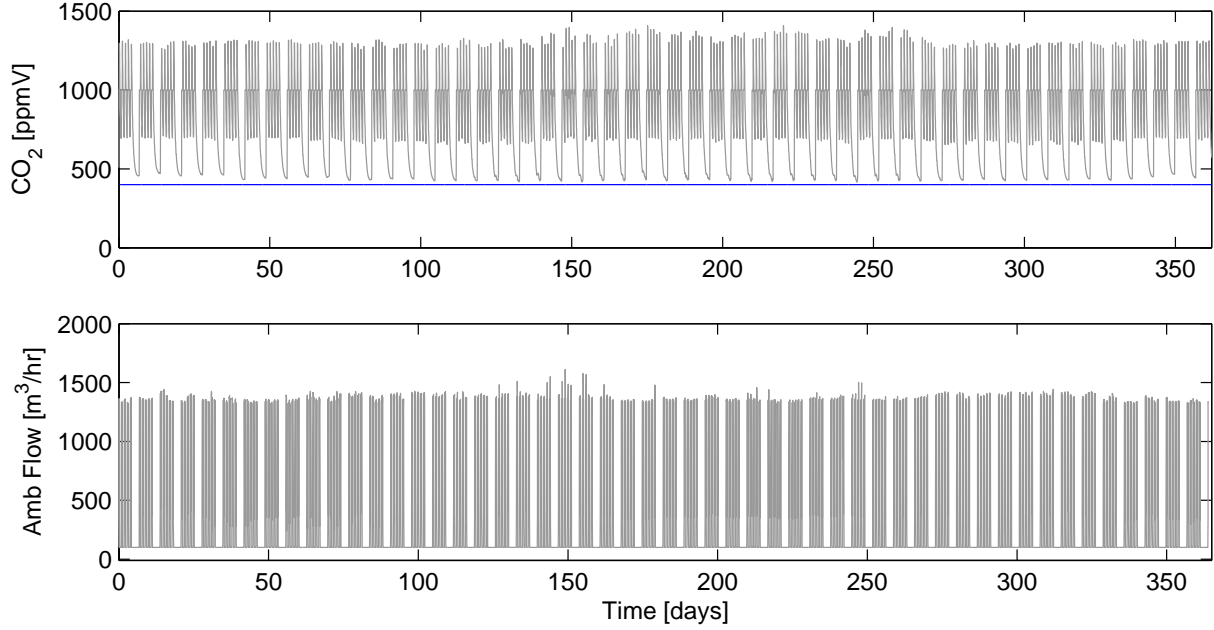


Figure 10: Trends for CO₂ concentration (solid line is ambient concentration) under building-wide optimization strategy (top). Profiles for ventilation rate (bottom).

CO₂ concentration since temperature changes expand and contract the building internal air mass. Consequently, multivariable interactions can be exploited to control air quality. This is important since this gives the system to use the ventilation rate to save energy and not only to maintain air quality.

5.1.3 Effects of Humidity and Pressure

To analyze the effect of humidity constraints on energy savings, we ran a scenario in which the comfort conditions for relative humidity are restricted to the range 40 – 50% during occupied times. We compare this with the relaxed range of 30 – 50%. In both scenarios, a range of 20 – 70% is used under unoccupied times. The year-round energy consumption for the tight comfort range is 225.54 MWh, whereas that of the relaxed range (base case) is 225.17 MWh. The difference is negligible. We also found that not relaxing the relative humidity constraints during unoccupied times increases energy consumption to 226.82 MWh, an increase of 0.8% with respect to relaxed case. This negligible effect can be explained from the ability of the building to limit external ventilation and from the dependence of the building relative humidity on temperature. In particular, from (2.6) and (2.7), we can see that the relative humidity inside the building can be *partially* controlled not only by modifying the water content (C_{H_2Oz}) through the cooling coil but also by adjusting the the saturation concentration $C_{H_2O}^{sat}(\tau)$ by adjusting the building temperature. In particular, the saturation concentration is highly sensitive to temperature. Consequently, by allowing the temperature to vary across the comfort zone, more flexibility in relative humidity control can also be obtained, and less energy is used in the cool-

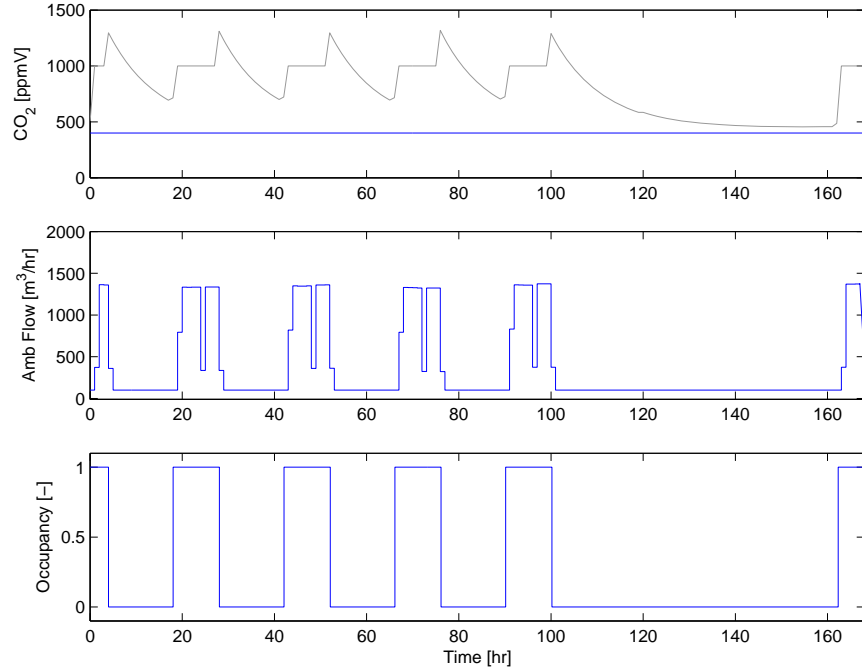


Figure 11: Trends for CO₂ concentration (top), ventilation rate (middle) and occupancy status (bottom) during a week of operation.

ing coils. The building-wide strategy thus avoids the limitations of traditional single-loop control systems that use exclusively the cooling coil to control relative humidity by adjusting absolute humidity. It is important to highlight that most sensors and comfort conditions are based on relative humidity (as opposed to absolute humidity which is a measure of water content). Consequently, from a comfort point of view, it makes sense to control relative humidity.

We performed a similar analysis to evaluate the effect of pressure constraints. We ran a scenario with a tight pressure range of 1-1.1 atm. tight pressure constraints are desired to avoid building infiltration effects. We compared this scenario with a relaxed range of 0.9-1.2 atm. The relaxed range resulted in an energy consumption of 225.17 MWh, whereas the energy consumption with tight pressure constraints was 234.4 MWh which represents a non-negligible increase of 4% in energy consumption. This was an unexpected result since pressure is normally not considered as a variable that can be used to achieve energy savings. From the ideal gas law (2.5) we can see that at constant building mass, imposing constraints on pressure implicitly imposes a constraint on temperature. In other words, tightening the pressure bounds limits flexibility to move the temperature within the comfort zone. In addition, as mentioned previously, pressure is an indirect variable that can be used to optimize air quality.

5.1.4 Effects of Occupancy Detection

Detecting the occupancy status of the building has significant effects on energy consumption. To quantify this effect, we analyzed the case in which the change in occupancy status is detected with

a delay of a single hour in the afternoon. This leads to an extra operation hour at 6-7 p.m and a year-round energy consumption of 229.53 MWh compared with the base case of 225.17 MWh. This represents an increase of 2%.

Another way of quantifying the impact of detecting occupancy is by using the same limits for temperature, pressure, CO₂ and humidity in occupied and unoccupied mode. In this scenario, the energy consumption goes up to 345 MWh (energy savings decrease to 77%). This demonstrates that exploiting unoccupancy periods is an important variable driving energy savings. Interestingly, the magnitude of the change again confirms the more critical role of the exploiting the thermal comfort zone.

5.1.5 Effects of Degrees of Freedom

Besides the ventilation rate q^{amb} , the comfort zone and occupancy, the delivery conditions of the AHU (temperature $T^{z,in}$ and inlet flow $q^{z,in}$) provide flexibility for saving energy. To illustrate the effect of the inlet temperature, we consider the case where the delivery temperature range is tightened from 15 – 28°C to 18 – 27°C. The energy consumption increases to 225.30 MWh, which is negligible compared to the base case of 225.17 MWh. The explanation is that the constraint on the inlet flow never becomes active so it can always compensate for the tighter inlet temperature constraint. If we tighten the ramp limit for the inlet flow (3.19a) from 5000 m³/hr² to 500 m³/hr² the energy consumption goes up to 240 MWh, an increase of 6.6% with respect to base case. If we also tighten the ramp limits on the ventilation rate (3.19d) from 1000 m³/hr² to 100 m³/hr² and tighten the limit of the inlet flow to 100 m³/hr, the energy consumption increases to 241 MWh. As can be seen, ramp constraints can indeed limit energy savings since they affect the responsiveness of the system. This information is of practical importance because dampers have slow dynamics. We observe, however, that the magnitude of the impact is not significant.

One of the general conclusions from the previous analysis is that the energy savings of the building-wide strategy are not particularly sensitive to flow, CO₂, and humidity constraints. This implies that, from a building-wide point of view, the thermal comfort zone, ventilation rates, and the unoccupancy periods *provide enough flexibility* to achieve significant energy savings.

5.2 Comfort-Energy Trade-Off

A multi-objective framework can be used to trade-off between energy consumption and comfort. In Figure 12, we present a Pareto front of energy consumption against comfort error for 3 days of operation. Here, comfort is measured as the squared error from a desired reference point of 22°C and 50% relative humidity as in equation (4.24). We scaled the error to stay within the range 0-10.

The proposed utopia-tracking strategy of Section (4.2) locates the utopia point and the compromise solution to compute the optimal trade-off point at the current real-time conditions. This is of practical important since, as we can see from Figure 12, the Pareto curve is steep at tight comfort conditions (e.g., a small change in comfort translates in large amounts of energy). This observation gives another explanation for the large energy savings of the building-wide strategy compared to the tracking strategy. In particular, tracking comfort strictly (minimizing comfort error) leads to a

very high energy consumption. From the graph, we can see that a comfort error of around 0.2 gives an energy consumption of nearly 5,000 kW while increasing allowing a small drift of the error (i.e., drift from $22^{\circ}C$) can bring down the energy consumption to levels of 2,500 kWh. This gives energy savings of 50%. The impact of allowing temperature drifts from fixed comfort set-points on energy savings has also been analyzed in [30].

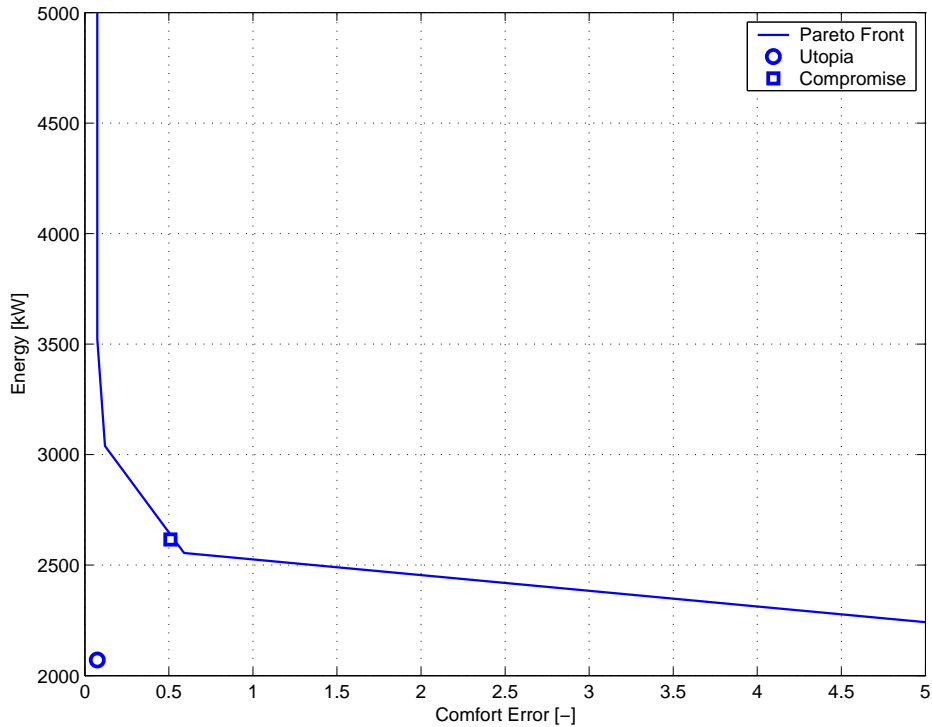


Figure 12: Comfort-energy Pareto front, utopia point, and compromise solution.

We can conclude that exploiting the comfort zone constraints as opposed to using a competing comfort objective with set-point tracking leads to much higher energy savings. To illustrate this, we ran a building-wide optimization scenario tightening the comfort limits from $21 - 27^{\circ}C$ to $23 - 27^{\circ}C$ during occupied conditions. This tighter temperature range corresponds to a PMV index of 0.5 and a PPD value of 8%. In this case, the year-round energy consumption goes to 250 MWh (savings go down to 83% compared to the tracking strategy). Interestingly, the energy savings compared with those of the tracking strategy are still significant indicating that tight comfort ranges can be achieved. The key again is to avoid the tracking of fixed set-points.

5.3 Economic Performance

We analyzed the economic performance of the building-wide strategy under day-ahead $\lambda_D(\tau)$ and real-time prices $\lambda_R(\tau)$. For comparison, we first evaluated the operating policy under direct energy minimization with both price trends *using strictly positive prices* (we bound the prices from below at a value of $10\$/MWh$). We found that the annual cost under day-ahead prices was $\$6.25 \times 10^4$ while

that under real-time prices was $\$6.0 \times 10^4$. The cost profiles are presented in Figure 13. Note that even if real-time prices lead to large cost spikes during the summer, the costs during the winter are lower thus leveling out the year-round effect. In fact, the total cost is lower under real-time prices, which was unexpected.

We also run the system using an economic objective function (??) under the day-ahead and real-time prices. We found that the annual cost under day-ahead prices was $\$6.24 \times 10^4$ while that under real-time prices was $\$5.98 \times 10^4$. As can be seen, the differences with the energy minimization strategy are negligible. This result is surprising, since it is commonly believed that demand-shifting strategies can lead to significant cost reductions. The results presented here provide a counterexample to this perception.

We found that if a shorter prediction horizon of 12 hours is used, the costs under cost minimization with real-time prices go up to $\$6.13 \times 10^4$ while the costs under day-ahead prices remain unchanged. If the horizon is decreased further to 11 hours, the problem becomes infeasible under real-time pricing (ramp constraints limit responsiveness). We can conclude that, *under high price variability and decreased predictability*, operations become more sensitive to foresight since the building cannot react instantaneously [3]. This is important because real-time prices are extremely difficult to forecast. This sensitivity to foresight does not occur under day-ahead prices, since they are more steady. Consequently, it is preferable to minimize energy consumption directly or to bid into day-ahead markets.

We analyzed a second scenario in which we allow prices to be negative. For the energy minimization strategy, the year-round energy consumption was 230 MWh. The cost under real-time prices was $\$5.88 \times 10^4$. The cost minimization strategy under real-time prices was $\$4.90 \times 10^4$, a reduction of 20% with respect to the energy minimization strategy. The energy consumption, however, increased to 285 MWh, an increase of 19%. This clearly indicates the trade-off between energy costs and demand. Under day-ahead prices the cost was $\$6.24 \times 10^4$ and the energy demand was 235 MWh. The costs for the day-ahead and real-time prices are presented in Figure 14. We can see that day-ahead prices do not provide financial incentives throughout the year since prices remain positive. Finally, we have found that, under real-time prices with negative values, the volatility of operations under the cost minimization strategy increases significantly since the system tries to move quickly to exploit the negative price spikes thus losing responsiveness. In particular, infeasibility problems were often observed for horizons of less than 12 hours.

A conclusion from this study is that buildings do not benefit from following economic objectives if no financial incentives are provided. Negative prices typically observed in real-time markets provide strong incentives but they are extremely difficult to predict. Consequently, exploiting the building dynamics to shift demands in a proactive manner is complicated. In addition, highly volatile prices lead to unstable operations and infeasibility.

Since energy minimization and day-ahead formulations reach nearly identical costs, buildings do not seem to benefit from participating in existing day-ahead electricity markets and, consequently, from providing demand forecast information. The ISO, however, benefits significantly from having better estimates of demand in clearing day-ahead markets since it leads to higher market efficiency and grid reliability. Consequently, the question remains open as to *what is the right market design*

providing financial incentives for buildings. In particular, it seems that buildings should profit from providing ancillary services such as forecast information, regulation, storage, and ramping capacity. While demand response programs can provide a financial incentive, current sporadic events are insufficient.

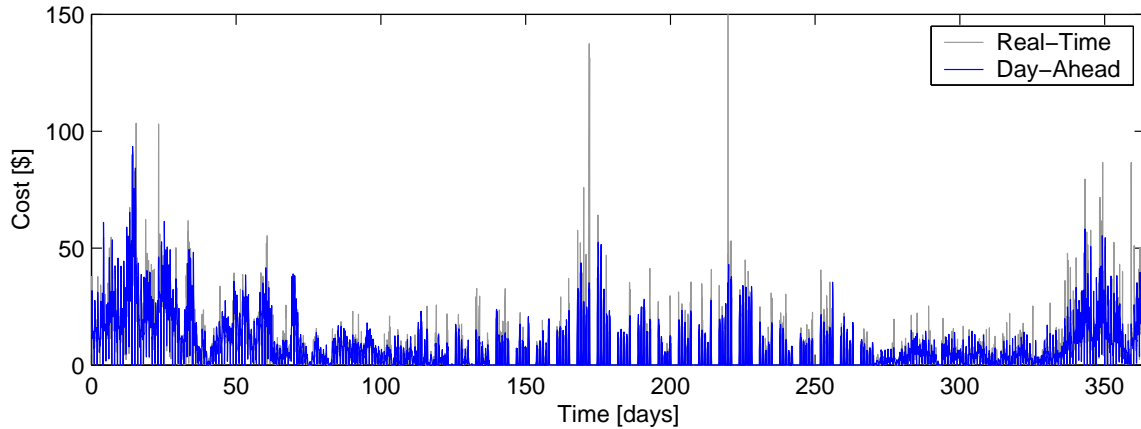


Figure 13: Cost profiles under day-ahead and real-time prices with strictly positive prices.

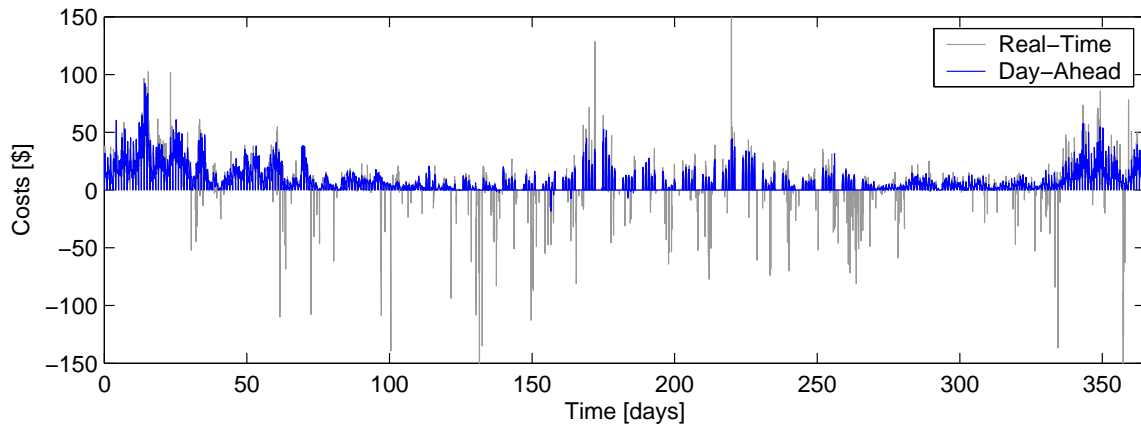


Figure 14: Cost profiles under day-ahead and real-time prices allowing for negative prices.

6 Conclusions and Future Work

In this work, we have presented strategies for building-wide optimization in real-time environments. We have found that physical interactions among CO_2 , temperature, pressure, humidity and occupancy provide significant flexibility to achieve significant energy savings without sacrificing air quality and comfort. Our analysis indicates that the exploitation of the thermal comfort zone is the most relevant factor driving energy savings beyond 50%. In addition, we have presented different strategies to deal with complex pricing functions and interactions with electricity markets. In this context,

we have found that direct energy minimization instead of cost minimization is a more reliable strategy under highly volatile market prices with no financial incentives. In the presence of financial incentives given by negative real-time prices cost minimization can lead to substantial savings compared to energy minimization. Real-time prices, however, are difficult to anticipate and follow due to the slow dynamics of the building.

As part of future work, we will add higher-fidelity models and explore observability issues due to limited CO₂ and occupancy sensor information. In addition, we will seek strategies to price ancillary services provided by commercial buildings and we will analyze the effect of different market designs.

Acknowledgments

This work was supported by the U.S. Department of Energy, under Contract No. DE-AC02-06CH11357. Financial support from the Office of Energy Efficiency and Renewable Energy of the U.S. Department of Energy is also acknowledged. The author thanks Tom Celinski and Michael Zimmerman of BuildingIQ as well Marvin Kirshenbaum of Argonne National Laboratory for technical discussions.

A Model Nomenclature

A.1 Variables

$m^z(\cdot)$	total air mass in the building, gr_{air}
$C_i^z(\cdot)$	concentration of component i in building air, gr_i/m^3
$C_i^{in,z}(\cdot)$	concentration of component i in inlet air, gr_i/m^3
$C_i^m(\cdot)$	concentration of component i in mixer, gr_i/m^3
$m_i^{rm}(\cdot)$	mass removal rate of component i in AHU, gr_i/hr
$P^z(\cdot)$	building pressure, atm
$ppmV_{CO_2}^z(\cdot)$	CO ₂ concentration, $ppmV$
$q^{in,z}(\cdot)$	volumetric inlet flow rate, m^3/hr
$q^{out,z}(\cdot)$	volumetric outlet flow rate, m^3/hr
$q^m(\cdot)$	volumetric flow rate in mixed, m^3/hr
$q^{amb}(\cdot)$	volumetric ambient air flow rate, m^3/hr
$q^{ex}(\cdot)$	volumetric exhaust air flow rate, m^3/hr
$Q^{lat}(\cdot)$	latent heat removed in AHU, kJ/hr
$Q^{sens}(\cdot)$	sensible heat removed in AHU, kJ/hr
$Q^{hvac}(\cdot)$	electrical energy consumed by HVAC, kJ/hr
$T^z(\cdot)$	average temperature in building, K
$T^{in,z}(\cdot)$	temperature of inlet air, K
$T^m(\cdot)$	temperature in mixer, K
$RH^z(\cdot)$	relative humidity in building, %

A.2 Data

$C_i^{amb}(\cdot)$	concentration of component i in ambient air, gr_i/m^3
$T^{amb}(\cdot)$	temperature of ambient air, K
n_{tot}	number of occupants, 500
G_i^z	generation rate of component i per occupant, ($CO_2 = 2.4, H_2O = 50$) gr_i/hr [2]
Q^z	building heat gain per occupant, $432 kJ/hr$
U^w	wall heat-transfer coefficient, $18 kJ/hr \cdot m^2 \cdot K$ [24]
V^z	total building volume, $1000 m^3$
A^w	total wall heat-transfer area, $600 m^2$
c_p	air heat capacity at standard conditions, $1.0 \times 10^{-3} kJ/gr_{air} \cdot K$ [23]
h^{lat}	latent heat of condensation, $2.46 kJ/gr_{H_2O}$ [22]
ρ	air density at standard conditions, $1200 g/m^3$ [23]
M	air molecular weight, $29 gr/gr_{mol}$
M_{CO_2}	CO_2 molecular weight, $44 gr/gr_{mol}$
R	universal gas constant, $0.082 \times 10^{-3} atm \cdot m^3/gr_{mol}K$

References

- [1] EPA on-line tools for site assessment calculation, 2011.
- [2] H. Aglan. Predictive model for CO_2 generation and decay in building envelopes. *Journal of Applied Physics*, 93:1287–1290, 2003.
- [3] V. M. Zavala and J. Wang, S. Leyffer, E. M. Constantinescu, M. Anitescu, and G. Conzelmann. Proactive energy management for next-generation building systems. *In Proceedings of 4th International Conference of IBPSA-USA*, 2010.
- [4] J. E. Braun. Reducing energy costs and peak electricity demand through optimal control of building thermal storage. *ASHRAE Transactions*, 96(2):876–888, 1990.
- [5] J. E. Braun, K. W. Montgomery, and N. Chaturvedi. Evaluating the performance of building thermal mass control strategies. *HVAC&Research*, 7(4):403–428, 2001.
- [6] T. Y. Chen. Real-time predictive supervisory operation of building thermal systems with thermal mass. *Energy and Buildings*, 33(2):141 – 150, 2001.
- [7] T. Y. Chen. Application of adaptive predictive control to a floor heating system with a large thermal lag. *Energy and Buildings*, 34(1):45 – 51, 2002.
- [8] A. Chinchuluun and P. M. Pardalos. A survey of recent developments in multiobjective optimization. *Annals of Operations Research*, 154:29–50, 2007.
- [9] D. B. Crawley, L. K. Lawrie, C. O. Pedersen, R. J. Liesen, D. E. Fisher, R. K. Strand, R. D. Taylor, R. C. Winkelmann, W. F. Buhl, Y. J. Huang, and A. E. Erdem. EnergyPlus: A new-generation

- building energy simulation program. In *Proceedings of Building Simulation '99*, volume 1, pages 81–88, 1999.
- [10] M. Diehl, H. J. Ferreau, and N. Haverbeke. Efficient numerical methods for nonlinear MPC and moving horizon estimation. In *Nonlinear Model Predictive Control*, pages 391–417, 2009.
- [11] K.F. Fong, V.I. Hanby, and T.T. Chow. HVAC system optimization for energy management by evolutionary programming. *Energy and Buildings*, 38(3):220 – 231, 2006.
- [12] K.F. Fong, V.I. Hanby, and T.T. Chow. System optimization for hvac energy management using the robust evolutionary algorithm. *Applied Thermal Engineering*, 29(11-12):2327 – 2334, 2009.
- [13] R. Fourer, D. Gay, and B. Kernighan. *AMPL*. The Scientific Press, South San Francisco, 1993.
- [14] A. Gambier. MPC and PID control based on multi-objective optimization. *Proceedings of the American Control Conference*, pages 4727–4732, 2008.
- [15] Y. Ke and S. Mumma. Using carbon dioxide measurements to determine occupancy for ventilation controls. *ASHRAE Transactions*, 103:365–374, 1997.
- [16] M. Kintner-Meyer and A. F. Emery. Optimal control of an HVAC system using cold storage and building thermal capacitance. *Energy and Buildings*, 23(1):19 – 31, 1995.
- [17] S. A. Klein, J. A. Duffie, and W. A. Beckman. TRNSYS: A transient simulation program. *ASHRAE Transactions*, 82:623–633, 1976.
- [18] D. Kolokotsa, A. Pouliezios, G. Stavrakakis, and C. Lazos. Predictive control techniques for energy and indoor environmental quality management in buildings. *Building and Environment*, 44(9):1850 – 1863, 2009.
- [19] F. Oldewurtel, A. Parisio, C. N. Jones, M. Morari, D. Gyalistras, M. Gwerder, V. Stauch, B. Lehmann, and K. Wirth. Energy efficient building climate control using stochastic model predictive control and weather predictions. *Proceedings of American Control Conference*, pages 5100–5105, 2010.
- [20] B. W. Olesen and G. S. Brager. A better way to predict comfort: The new ASHRAE standard 55-2004. *ASHRAE Journal*, pages 20–26, 2004.
- [21] B. Paris, J. Eynard, S. Grieu, T. Talbert, and M. Polit. Heating control schemes for energy management in buildings. *Energy and Buildings*, 42(10):1908 – 1917, 2010.
- [22] R. H. Perry and D. W. Gree. *Perry's Chemical Engineer's handbook*. McGraw-Hill, 2007.
- [23] R. .C. Reid, J. M. Prausnitz, and B. E. Poling. *The properties of gases and liquids*. McGraw-Hill, 1987.
- [24] Bourhan Tashtoush, M. Molhim, and M. Al-Rousan. Dynamic model of an HVAC system for control analysis. *Energy*, 30(10):1729 – 1745, 2005.

- [25] A. Wächter and L. T. Biegler. On the implementation of a primal-dual interior point filter line search algorithm for large-scale nonlinear programming. *Mathematical Programming*, 106:25–57, 2006.
- [26] Shengwei Wang and Xinqiao Jin. Model-based optimal control of VAV air-conditioning system using genetic algorithm. *Building and Environment*, 35(6):471 – 487, 2000.
- [27] J. K. Ward, J. Wall, S. West, and R. de Dear. Beyond comfort managing the impact of HVAC control on the outside world. In *Proceedings of Conference: Air Conditioning and the Low Carbon Cooling Challenge*, 2008.
- [28] V. M. Zavala and L. T. Biegler. Nonlinear programming strategies for state estimation and model predictive control. In *Nonlinear Model Predictive Control*, pages 419–432, 2009.
- [29] V. M. Zavala, E. M. Constantinescu, M. Anitescu, and T. Krause. On-line economic optimization of energy systems using weather forecast information. *Journal of Process Control*, 19:1725–1736, 2009.
- [30] V. M. Zavala, D. Skow, T. Celinski, and P. Dickinson. Techno-economic evaluation of a next-generation building energy management system. *Technical Report ANL/MCS-TM-313, Argonne National Laboratory*, 2011.

The submitted manuscript has been created by UChicago Argonne, LLC, Operator of Argonne National Laboratory (“Argonne”). Argonne, a U.S. Department of Energy Office of Science laboratory, is operated under Contract No. DE-AC02-06CH11357. The U.S. Government retains for itself, and others acting on its behalf, a paid-up, nonexclusive, irrevocable worldwide license in said article to reproduce, prepare derivative works, distribute copies to the public, and perform publicly and display publicly, by or on behalf of the Government.